Quantum metrology with one-dimensional superradiant photonic states

V. Paulisch,[1,*] M. Perarnau-Llobet,[1,*] A. González-Tudela,[1,2,†] and J. I. Cirac[1]
[1]*Max-Planck-Institut für Quantenoptik, Hans-Kopfermann-Str. 1, D-85748 Garching, Germany*
[2]*Instituto de Física Fundamental IFF-CSIC, Calle Serrano 113b, Madrid 28006, Spain*

(Received 23 May 2018; revised manuscript received 17 September 2018; published 8 April 2019)

Photonic states with large and fixed photon numbers, such as Fock states, enable quantum-enhanced metrology but remain an experimentally elusive resource. A potentially simple, deterministic, and scalable way to generate these states consists of fully exciting N quantum emitters equally coupled to a common photonic reservoir, which leads to a collective decay known as Dicke superradiance. The emitted N-photon state turns out to be a highly entangled multimode state, and to characterize its metrological properties in this work we (i) develop theoretical tools to compute the quantum Fisher information of general multimode photonic states, (ii) use it to show that Dicke superradiant photons in one-dimensional waveguides achieve Heisenberg scaling, which can be saturated by a parity measurement, and (iii) study the robustness of these states to experimental limitations in state-of-the-art atom-waveguide QED setups.

DOI: 10.1103/PhysRevA.99.043807

I. INTRODUCTION

Quantum metrology exploits quantum resources, such as squeezing and entanglement, to enhance the precision of measurements beyond the capabilities of any classical scheme [1–4]. Given N probes to estimate an unkown parameter φ, classical measurements are limited by the shot-noise limit (SNL) $\Delta\varphi = 1/\sqrt{N}$, whereas entangled probes can surpass this bound possibly reaching the Heisenberg limit (HL), $\Delta\varphi = 1/N$, which in fact provides the ultimate bound on sensitivity. In atomic ensembles, achieving quantum-enhanced metrology with relatively large particle numbers appears possible [5–13]. The situation becomes more challenging when dealing with photonic states in optical interferometry. Squeezed states, a well-known resource [14], are very challenging to scale up, with current demonstrations being at the few-photon level [15,16]. States with a well-defined photonic number, e.g., NOON [17] and twin-Fock [18] states, also constitute a powerful resource, which has been experimentally tested for few-photon states [19–21]. Yet, current experimental methods to generate these states are limited by both low fidelities and efficiencies, since they are based in combining heralded single photons with postselection, which naturally leads to an exponential decrease of the efficiency with increasing N [22,23].

A promising approach for generating multiphoton states in a deterministic, efficient, and scalable manner are quantum emitters coupled to photonic waveguides [24–32]. In these setups, the waveguide decay rate, Γ_{1d}, can exceed the free space one, Γ^*, and naturally enhance the photon collection efficiency of the system. On top of that, when all the quantum emitters couple equally to the waveguide, their dynamics is described by the celebrated Dicke model [33], which predicts an additional collective enhancement of the waveguide decay rate. Given N emitters in the waveguide and m collective atomic excitations, previous studies focused on the regime $m \ll N$ [34], where the m collective excitations decay into a single-mode m-photon wave packet with an error scaling as $\varepsilon_{\text{lin}} \sim m\Gamma^*/(N\Gamma_{1d})$. The main limitation of this regime arises in the preparation of the initial state, since creating a fixed number m of collective atomic excitations requires the use of sophisticated protocols [35–37].

A conceptually and experimentally simpler approach consists of exciting all the quantum emitters, i.e., $m = N$. In this regime, the emitters experience a nonlinear decay, known as Dicke superradiance, leading to a multimodal structure of the emitted N-photon wave packet [35], which can be generally written as

$$|\phi_A^{(N)}\rangle = \int\cdots\int \frac{dk_1\ldots dk_N}{(2\pi)^N N!} A_{\{k\}} a_{k_1}^\dagger \ldots a_{k_N}^\dagger |0\rangle, \qquad (1)$$

where $a_{k_i}^\dagger$ is the creation operator of a waveguide photon of momentum k_i. The coefficient $A_{\{k\}} = A_{k_1,k_2,\ldots,k_n}$ characterizes the multimodal structure of the wave packet. In contrast to the case of linear decay processes [34], it is not factorizable: $A_{\{k\}} \neq \sqrt{N!}A_{k_1}\cdots A_{k_n}$. This protocol uses all possible excitations while having a particularly simple initial state, making it very attractive for experiments. However, the multimode form of the emitted state prevents the direct use of previous results in quantum optical metrology [1–4]. In fact, the potential of Dicke superradiant states for metrology has not been addressed so far, despite being a promising candidate.

In this work, we show that one-dimensional Dicke superradiant states achieve Heisenberg scaling as $[\Delta\varphi]_{\text{Dicke}} \approx 0.41/N$, performing only slightly worse than Fock states, $[\Delta\varphi]_{\text{Fock}} \approx 0.5/N$. Furthermore, we characterize the robustness of Dicke superradiant states to several experimental error sources, showing how they are particularly robust to photon losses with an error scaling as $\varepsilon_{\text{nl}} \propto \ln(N)\Gamma^*/\Gamma_{1d}$, for $\Gamma_{1d} \gg \Gamma^*$. Thus, for a given ratio Γ_{1d}/Γ^*, and desired

*These authors contributed equally to this work.
†a.gonzalez.tudela@csic.es

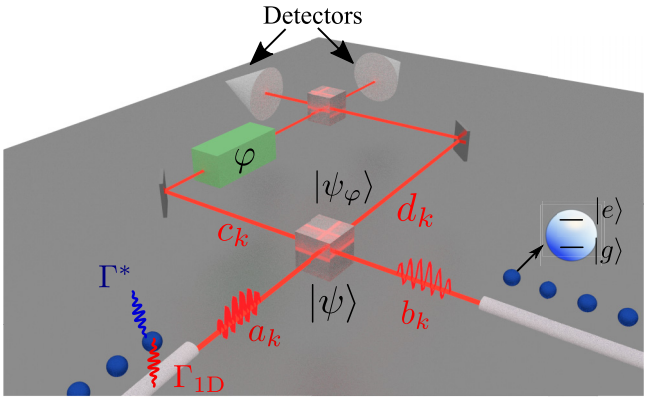

FIG. 1. General scheme of the protocol: two emitter ensembles are coupled collectively to two waveguides connected to the A/B ports of a Mach-Zehnder interferometer.

error, $\varepsilon_{\rm nl}$, our protocol can potentially generate up to $N \sim \exp(\varepsilon_{\rm nl}\Gamma_{1d}/\Gamma^*)$ photons, paving the way for efficient and scalable quantum-enhanced metrology protocols. To obtain these results, we develop theoretical tools to characterize the metrological properties of general multimode states of the form (1) in Mach-Zender interferometry. We illustrate their potential in multimodal photonic states created in anharmonic cavities [38], which we show to allow for quantum-enhanced metrology without reaching Heisenberg scaling, and envisage they can be readily applied to other multimode states that appear in relevant experimental setups, such as biexciton emission in quantum dots [39].

II. QUANTUM OPTICAL INTERFEROMETRY

A paradigmatic task in optical interferometry is the measurement of a phase φ with high precision. The standard setup is the so-called Mach-Zehnder interferometer depicted in Fig. 1. The main resource of this protocol is the initial photonic state, $|\psi\rangle$, impinging onto the first beam splitter with input (output) ports A/B (C/D) with annihilation operators a/b (c/d). The beam splitter can be described as a unitary $\bar{U}_{BS}(\theta) = \exp[\theta(a^\dagger b - b^\dagger a)]$ with the mixing angle θ. After this operation the photon can travel in two different arms, acquiring a relative phase φ through $\bar{U}_\varphi = \exp[-i\varphi/2(c^\dagger c - d^\dagger d)]$. This results in a state $|\psi_\varphi\rangle$, which now contains information on φ. By applying a measurement M on $|\psi_\varphi\rangle$, the phase φ can be estimated with an uncertainty $\Delta\varphi$. In general, $\Delta\varphi$ depends on $|\psi_\varphi\rangle$, M, and the number of repetitions of the experiment ν. Assuming $\nu \gg 1$, the quantum Cramér-Rao bound [40,41] gives a lower bound for $\Delta\varphi$ that is independent of M, $(\Delta\varphi)^2 \geqslant 1/\nu F_Q[\psi_\varphi]$, where $F_Q[\psi_\varphi]$ is the quantum Fisher information (QFI) [42] of the state $|\psi_\varphi\rangle$,

$$F_Q[\psi_\varphi] = 4(\langle\dot{\psi}_\varphi|\dot{\psi}_\varphi\rangle - |\langle\dot{\psi}_\varphi|\psi_\varphi\rangle|^2). \tag{2}$$

The QFI characterizes the potential of $|\psi_\varphi\rangle$ for estimating φ with an optimal measurement.

Let us illustrate the power of the QFI, with relevant examples in optical interferometry. For example, in classical sources using coherent states, $|\psi^{\rm cl}\rangle = |\alpha\rangle_A \otimes |0\rangle_B$, the QFI is at most proportional to the average photon number, $F_Q \leqslant \bar{N}$, with $\bar{N} = |\alpha|^2$. The upper bound of the QFI, given by the HL, $F_Q = N^2$, is obtained by NOON states [17], $|\psi_\varphi^{\rm NOON}\rangle = \frac{1}{\sqrt{2}}(|N0\rangle + |0N\rangle e^{iN\varphi})$, where $|N_u N_l\rangle$ indicates the number of photons in the C/D path. The more experimentally friendly twin-Fock states (TFS) [18], $|\psi_\varphi^{\rm TFS}\rangle = \bar{U}_\varphi \bar{U}_{BS}(\pi/4)|N/2\rangle_A \otimes |N/2\rangle_B$, obtained when two Fock states enter into the first beam splitter, also lead to Heisenberg scaling with slightly worse slope,

$$F_Q\big[\psi_\varphi^{\rm TFS}\big] = \frac{N(N+2)}{2}. \tag{3}$$

Furthermore, this bound can be saturated by a number-resolved measurement [43] or a parity [44] measurement, which is optimal for any bosonic state that is mode-symmetric [45]. Many other two-mode quantum states enable quantum-enhanced metrology (see, e.g., Refs. [46–48]), notably including random bosonic states [49]. In the following section, we go beyond the standard two-mode interferometry described above (see, e.g., the review [4]), and analyze the QFI when the input states of the interferometer are multimode states of the general form (1).

III. QUANTUM FISHER INFORMATION OF MULTIMODE STATES

Let us restrict our attention to the case where the initial state $|\psi\rangle = |\phi_A^{N_A}\rangle \otimes |\phi_B^{N_B}\rangle$ has a well-defined photon number $N_{A/B}$ at the A/B ports of the first beam splitter. The total photon number $N = N_A + N_B$ is the metrological resource. The states have the multimodal structure (1) with modal coefficients $A_{\{k\}}/B_{\{q\}}$, and where $\{k\} = \{k_1, \ldots, k_{N_A}\}$ and $\{q\} = \{q_1, \ldots, q_{N_B}\}$ represent the internal degrees of freedom of the A/B wave packet. In our case they are the momenta of the photons in the A/B wave packets, although the problem is generally formulated.

Generalizing the beam splitter and phase operation to deal with multimode variables:

$$U_{\rm BS}(\theta) = \exp\left[\int \frac{dk}{2\pi}(a_k^\dagger b_k - b_k^\dagger a_k)\theta\right] \tag{4}$$

and

$$U_\varphi = \exp\left[-i\frac{\varphi}{2}\int \frac{dk}{2\pi}(c_k^\dagger c_k - d_k^\dagger d_k)\right], \tag{5}$$

we consider states of the form $|\psi_\varphi^{\rm AB}\rangle = U_\varphi U_{\rm BS}(\pi/4)|\phi_A^{(N_A)}\rangle \otimes |\phi_B^{(N_B)}\rangle$. Exploiting the bosonic symmetry of the wave packets $A_{\{k\}}/B_{\{k\}}$ under permutation, we simplify the QFI of $|\psi_\varphi^{\rm AB}\rangle$ to a very transparent formula (see Appendix A 1),

$$F_Q\big[\psi_\varphi^{\rm AB}\big] = 2N_A N_B I_{AB} + N_A + N_B,$$

which only depends on a single integral I_{AB}:

$$I_{AB} = \int\cdots\int \frac{\prod_{i,j=1,1}^{N_A,N_B} dk_i dq_j}{(2\pi)^{N_A+N_B} N_A! N_B!} A^*_{k_1,\ldots,k_{N_A}} B^*_{q_1,\ldots,q_{N_B}} \times A_{q_1,k_2,\ldots,k_{N_A}} B_{k_1,q_2,\ldots,q_{N_B}}, \tag{6}$$

where the two indices k_1/q_1 have been exchanged in one of the coefficients. This formula is applicable to general multimode photonic states of a fixed photon number, and in the Appendix A 1 we extend it to situations where the number of photons is only fixed in one input of the interferometer. It is

easy to see that in the single-mode case $I_{AB} = 1$, in agreement with previous results [43]. Let us now focus on the case where the A/B wave packets have the same number of photons $N_A = N_B = N/2$ and the same modal structure $A_{\{k\}} = B_{\{k\}}$. These twin multimode states (TMS), denoted as $|\psi_\varphi^{\mathrm{TMS}}\rangle$, have a simple expression for the QFI,

$$F_Q\big[\psi_\varphi^{\mathrm{TMS}}\big] = \frac{N(I_N N + 2)}{2}, \tag{7}$$

where I_N is the integral of Eq. (6) for $N_A = N_B = N/2$ and $A_{\{k\}} = B_{\{k\}}$. Thus a general multimode wave packet will beat the SNL as long as I_N decays slower than $1/N$, and reach HL scaling if I_N tends to a constant. Importantly, in Appendix A 2 we show that the QFI saturates for a parity measurement. Now we compute I_N of two experimentally relevant photonic states, Dicke superradiant states, and photonic states generated in anharmonic cavities.

IV. QFI OF ONE-DIMENSIONAL SUPERRADIANT STATES

The first multimode photonic states that we consider are the ones naturally generated from N fully excited quantum emitters, described as two-level systems $\{|g\rangle, |e\rangle\}$, with an optical transition coupled to a waveguide mode at a rate $\Gamma_{1\mathrm{d}}$. We focus on the so-called mirror configuration [30–32], in which the emitter positions are fixed such that all of them interact equally with the waveguide modes. In that configuration, and assuming that the relaxation time scales of the waveguide are much faster than the time scales of the system dynamics [50], the quantum emitter dynamics are governed by the Dicke model [33]

$$\dot{\rho} = i(\rho H_{\mathrm{eff}}^\dagger - H_{\mathrm{eff}}\rho) + \Gamma_{1\mathrm{d}} S_{ge}\rho S_{eg}, \tag{8}$$

where ρ is the density matrix describing the quantum emitters' state, $H_{\mathrm{eff}} = \omega_0 S_{ee} - i\frac{\Gamma_{1\mathrm{d}}}{2} S_{eg}S_{ge}$ the effective non-Hermitian Hamiltonian, and where we denote the collective emitter operators as $S_{\alpha\beta} = \sum_j |\alpha\rangle_j\langle\beta|$.

Interestingly, if we initialize the system to be fully excited, $|e\rangle^{\otimes N}$, both the effective Hamiltonian and the quantum jump terms S_{ge}, S_{eg} restrict the evolution to the fully symmetric space. This guarantees that only N states participate in the evolution, which can be classified depending on their number of excitations, m, that we denote as $|\psi_m\rangle \propto S_{eg}^m |g\rangle^{\otimes N}$. From H_{eff}, note that these energy levels are linearly spaced, $\omega_m = m\omega_0$. The nonlinearity of the process emerges from the decay rates γ_m (associated to the transition $|\psi_m\rangle \to |\psi_{m-1}\rangle$) which depend on the number of excitations as $\gamma_m = m(N - m + 1)\Gamma_{1\mathrm{d}}$. In particular, $|\psi_m\rangle$ decays as $\gamma_m \propto N$ at the beginning and end of the process, while accelerating in the middle part, where $\gamma_{N/2} \propto N^2$, referred to as the Dicke superradiance effect. When all the emitters have decayed, the resulting photonic state reads [35]

$$A_{\{k\}} = \prod_{j=1}^{N} \frac{\sqrt{\gamma_j}}{i\big(j\omega_0 - \sum_{i=1}^{j}\omega_{k_i}\big) - \frac{1}{2}\gamma_j} + \{k_i \leftrightarrow k_j\}, \tag{9}$$

where we use the notation $\{k_i \leftrightarrow k_j\}$ to denote that the expression has to be symmetrized with respect to the momenta k_j. This wave packet inherits the nonlinearity from the decay process as temporal correlations between the N photons and, thus, it cannot be factorized as a single-mode one.

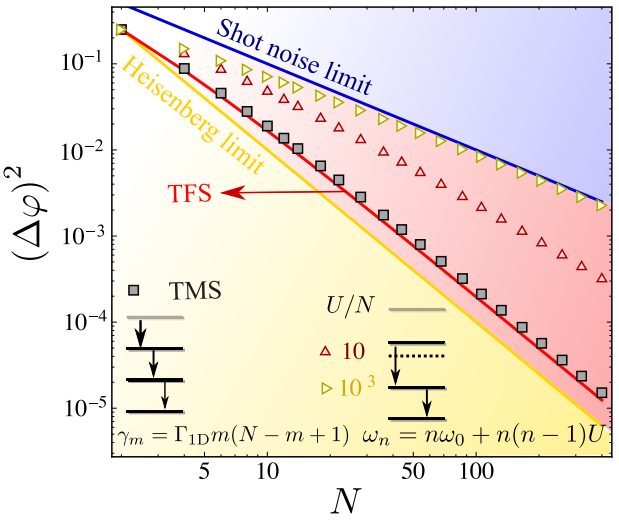

FIG. 2. Scaling of $(\Delta\varphi)^2$ with N for several situations discussed along the manuscript. In solid blue and yellow we plot both the shot-noise and Heisenberg limit (as depicted in the legend), respectively. In solid red, the scaling of Fock states. In black squares, we plot the numerical results for TMDS. In red (below) and yellow (upper) triangles. we plot the numerical results obtained of anharmonic cavities for $U/N = 10/10^3$ in $\Gamma_{1\mathrm{d}}$ units, respectively.

We now study the metrological potential of the states (9). For that, we consider a protocol where two ensembles with $N/2$ emitters are placed at the input ports of a Mach-Zehnder interferometer, as depicted in Fig. 1. Then, a simultaneous collective π pulse is implemented in both ensembles, leading to an emission of two heralded $N/2$-photon states: $|\phi_A^{(N/2)}\rangle$, $|\phi_B^{(N/2)}\rangle$. In principle, the wave packets are emitted in two directions but one can combine them such that they propagate in a single direction, while keeping the same metrological properties (see Appendix A 3). For obtaining the QFI of this state, we need to calculate the N-variable integral I_N for $A_{\{k\}}$ defined in Eq. (9). Note that there are $(N/2)!$ terms in (9), which lead to $[(N/2)!]^4$ terms in the integral. The number of integrals can always be reduced to $(N/2)^4$ by noting that all variables in I_N are exchangeable except for q_1 and k_1 [51]. For the $A_{\{k\}}$ in (9), we develop a recurrence relation which can be efficiently computed for large N, consisting of a multiplication of N matrices of at most size $3N \times 3N$ (see Appendix A 4). This allows for determining I_N exactly for large N. With this method, we numerically obtain that I_N quickly approaches a constant $I_N \approx 0.82$ for the range of N considered (up to ∼500 photons). This has the important consequence that the QFI of superradiant TMDS shows the Heisenberg scaling:

$$F_Q\big[\psi_\varphi^{\mathrm{TMDS}}\big] \approx 0.41N^2 + N. \tag{10}$$

where TMDS stands for twin multimode Dicke states. In Fig. 2, we plot $(\Delta\varphi)^2$ of $\psi_\varphi^{\mathrm{TMDS}}$ in black squares, together with Fock states (in solid red) showing how the multimodal case has the same scaling, just with a slightly reduced prefactor. This is the most important result of this work, since it provides

a path towards efficient and scalable multiphoton states useful for quantum metrology protocols.

V. EXPERIMENTAL CONSIDERATIONS

Since there are currently many platforms [24–32] with the potential to obtain superradiant photonic states, we analyze now the resilience of the QFI to several experimental imperfections in the preparation stage. We start by considering the main source of noise of these setups which comes from the emission into modes other than the waveguide ones, e.g., free space or a different waveguide polarization, that we embed into a single (individual) decay rate Γ^*. This term takes the states $|\psi_m\rangle$ out of the collective subspace at a rate $m\Gamma^*$, so that it is especially critical when the system is fully excited. The probability of emitting N-collective photons, which translates into a photon state fidelity, can be estimated as the probability of no jump in each step:

$$p \approx \prod_{m=1}^{N}\left(1-\frac{m\Gamma^*}{\gamma_m\Gamma_{1\mathrm{d}}}\right) \approx 1-\ln(N)\frac{\Gamma^*}{\Gamma_{1\mathrm{d}}}, \tag{11}$$

which is a valid assumption as long as $\Gamma_{1\mathrm{d}} \gg \Gamma^*\ln(N)$ and $N \gg 1$, like we numerically confirm through exact integration of the master equation (see Appendix A 5 a). The resulting photonic state will be a mixed state which can be written as $\rho_{N,*} = p|\phi_A^{(N)}\rangle\langle\phi_A^{(N)}| + (1-p)\sigma_1$, where σ_1 is a convex combination of state with less than N photons in the waveguide. Using two such mixed states as input of the interferometer, $\rho^{\mathrm{TMDS}} = \rho_{N/2,*}\otimes\rho_{N/2,*}$, we can bound its QFI by noting that the QFI is non-negative and additive under direct sum, obtaining

$$F_Q\big[\rho_\varphi^{\mathrm{TMS}}\big] \geqslant p^2 F_Q\big[\psi_\varphi^{\mathrm{TMS}}\big]. \tag{12}$$

This shows that, as long as we are in the limit $\Gamma_{1\mathrm{d}} \gg \Gamma^*$, the results become robust to photon loss with an error that increases only logarithmically with N.

Let us now enumerate other error sources, and provide the conditions under which they can be neglected (see Appendix A 5 for details). Absorption within the waveguide (or scattering through imperfections) provides a finite propagation length to the waveguide modes, L_{prop}, which spoils the collective behavior of the atomic interactions. To be able to neglect this effect the propagation length must be larger than the system size $L_{\mathrm{prop}} \gg N\lambda_a$, with λ_a being the wavelength of the waveguide modes determining the distance between QEs. State-of-the-art values for SiN waveguides [26] show $L_{\mathrm{prop}}/\lambda_a \sim 5\times10^4$, such that this will be in general a small correction. This finite lifetime of the waveguide modes also leads to photon loss, while the wave packet propagates away from the QEs. Furthermore, to neglect retardation effects, the propagation time scales, $\sim N\lambda_a/v_g$, must be much shorter than the shortest emitter time scale, that in this case occurs in the middle of the superradiant decay, being proportional to $(\Gamma_{1\mathrm{d}}N^2/4)^{-1}$.

Another error source is the deviation from the initial atomic state, e.g., by an imperfect control of the timing, T, or laser amplitude, Ω, in π pulse, that we embed in a single parameter $\Delta(\Omega T)$. If $\Delta(\Omega T)\sqrt{N} \ll 1$, this translates into a different initial state, $\approx(1-i\Delta(\Omega T)\sqrt{N}S_{ge})|e\rangle^{\otimes N}$, which leads to an error scaling as $\sim\Delta(\Omega T)^2N$. Other deviations from the ideal setting are that the two QE ensembles couple differently to the waveguide, $\Delta\Gamma_{1\mathrm{d}} = \Gamma_{1\mathrm{d}} - \Gamma_{1\mathrm{d}}^{'}$, or that the wave packets are emitted with a certain time delay, τ, rather than simultaneously. Both deviations decrease the integral I_N in the following way:

$$I_{N,\Delta\Gamma_{1\mathrm{d}}} \approx I_N\left(1-\frac{(\Delta\Gamma_{1\mathrm{d}})^2}{8\Gamma_{1\mathrm{d}}^2}N\right) \tag{13}$$

and

$$I_{N,\tau} \gtrsim I_N(1-N\Gamma_{1\mathrm{d}}\tau) \tag{14}$$

for $\Delta\Gamma_{1\mathrm{d}} \ll \Gamma_{1\mathrm{d}}$ and $N\Gamma_{1\mathrm{d}}\tau \ll 1$, respectively. Summarizing, one must ensure simultaneously that $N(\Delta\Gamma_{1\mathrm{d}})^2/\Gamma_{1\mathrm{d}}^2 \ll 1$ and $N\Gamma_{1\mathrm{d}}\tau \ll 1$ in order to guarantee quantum-enhanced metrology.

Finally, let us now briefly discuss imperfections in the interferometer and in the measurement. In Appendix A 5 f, we find that photon loss in the interferometer, quantified by a probability η, leads to a correction to the QFI that is smaller than $\eta N^2 I_N/4$ (at first order in η), so that one needs at most $\eta \ll 4.9N^{-2}$ to ensure Heisenberg scaling. For sufficiently large N, Heisenberg scaling is eventually lost with photon loss independent of the state into consideration. Then, the quantum advantage just shows up as a better prefactor in the scaling of the QFI with N [52,53]. This regime, which requires dealing with mixed states, will be discussed in a forthcoming publication [54], where we will show that TMDS of N photons have similar metrological properties to twin-Fock states of $\approx 0.91N$ photons. Given that twin-Fock states are known to be robust to photon loss, both in the interferometer [55] and in the measurement device [43], we expect TMDS to be a valuable resource for quantum-enhanced metrology in the presence of photon loss in the interferometer and in the apparatus [54].

VI. QFI OF ANAHARMONIC CAVITIES

Let us illustrate the potential of the tools we developed with another class of nonlinear photonic states appearing from anharmonic cavities [38], where the nonlinearity manifests as a nonlinear energy shift, i.e., $\omega_n = n\omega_0 + n(n-1)U$, while having linear decay rates $\gamma_n = n\gamma_1$. In Fig. 2 we plot the $(\Delta\varphi)^2$ for the photonic state emerging from the decay at the Nth level of the anaharmonic ladder for two values of U/γ_1. Interestingly, we observe that Heinseberg scaling is lost for any value of U, as we find numerically that $I_N \propto 1/N$ for large enough N. This is illustrated in Fig. 2 for $U/\gamma_1 = 10, 10^3$. This result shows that different multimode states can have completely different metrological properties, suggesting a rich relation between the multimode structure and the potential for metrology of the state. It also provides intuition on why TMDS behave similarly than TFS, since in that case all photons are spectrally centered at the same frequency ω_0, thus being mostly indistinguishable. More details on the relation between superradiant states and Fock states will be provided in a forthcoming publication [54].

VII. CONCLUSIONS

To sum up, we have proven that photons emitted from Dicke superradiant states [33] are useful for quantum metrology. To show it, we derive a computationally friendly way of calculating the QFI for arbitrary multimode photonic wave packets, illustrating its power with another physically relevant example (photons emitted from anharmonic cavities). The number of photons that can be produced for a fixed fidelity scales exponentially with Γ_{1d}/Γ^*. State-of-the-art nanophotonic setups [28] have already achieved ratios $\approx$60 with $\Gamma_{1d} \sim$ 1 GHz, which indicates the possibility of generating hundreds of photons at the level of 90% fidelities and GHz rates. Furthermore, most of the conclusions can be extrapolated to other systems where collective decays can be engineered, such as cavity QED setups [56–59]. We foresee other possible applications in situations where Fock states provide advantage, as it is the case in quantum lithography [60].

ACKNOWLEDGMENTS

We thank J. B. Brask, C. Gogolin, P. Hofer, J. Kołodyński, V. Sandoghdar, and J. Thompson for valuable discussions and comments on the manuscript. V.P. acknowledges the Cluster of Excellence Nano Initiative Munich (NIM). M.P.L. acknowledges the Alexander Von Humboldt Foundation. A.G.T. and I.C. acknowledge ERC Advanced Grant QENOCOBA under the EU Horizon 2020 program (Grant Agreement No. 742102).

APPENDIX

1. Derivation of the quantum Fisher information

To derive the quantum Fisher information of the TMS, we work in a more general setting of two different multimode states incident on the two ports of the first beam splitter. We write them as

$$\left|\phi_A^{(m)}\right\rangle = \int\!\dots\!\int \frac{dk_1 \dots dk_m}{(2\pi)^m m!} A_{k_1\dots k_m} a_{k_1}^\dagger \dots a_{k_m}^\dagger |0\rangle,$$

$$\left|\phi_B^{(n)}\right\rangle = \int\!\dots\!\int \frac{d\tilde{k}_1 \dots d\tilde{k}_n}{(2\pi)^n n!} B_{\tilde{k}_1\dots\tilde{k}_n} b_{\tilde{k}_1}^\dagger \dots b_{\tilde{k}_n}^\dagger |0\rangle.$$

Abusing notation, here we will also call the output modes of the interferometer a_k and b_k. Then, the state after the beam splitter and the phase operation, $|\psi_\varphi\rangle = U_\varphi U_{\rm BS}|\phi_A^{(m)}\rangle \otimes |\phi_B^{(n)}\rangle$, is given by

$$|\psi_\varphi\rangle = \int\!\dots\!\int \frac{\prod_{i,j=1}^{m,n} dk_i d\tilde{k}_j}{(2\pi)^{m+n} m!n!} A_{k_1\dots k_m} B_{\tilde{k}_1\dots\tilde{k}_n} c_{k_1}^\dagger \dots c_{k_m}^\dagger d_{\tilde{k}_1}^\dagger \dots d_{\tilde{k}_n}^\dagger |0\rangle, \tag{A1}$$

where we defined the creation operators $c_k^\dagger \equiv c_k^\dagger(\varphi) = U_\varphi U_{\rm BS} a_k^\dagger U_{\rm BS}^\dagger U_\varphi^\dagger = \frac{1}{\sqrt{2}}(e^{-i\varphi/2}a_k^\dagger + e^{i\varphi/2}b_k^\dagger)$, and respectively for $d_k^\dagger \equiv d_k^\dagger(\varphi) = \frac{1}{\sqrt{2}}(-e^{-i\varphi/2}a_k^\dagger + e^{i\varphi/2}b_k^\dagger)$.

For calculating the QFI of $|\psi_\varphi\rangle$ one has to take the derivative, which turns $c_k^\dagger$ ($d_k^\dagger$) into $\frac{i}{2}d_k^\dagger$ ($\frac{i}{2}c_k^\dagger$). This leads to

$$|\dot{\psi}_\varphi\rangle = \left(\frac{i}{2}\right)^{\frac{m+n}{2}} \int\!\dots\!\int \frac{\prod_{i,j=1}^{m,n} dk_i d\tilde{k}_j}{(2\pi)^{m+n} m!n!} A_{k_1\dots k_m} B_{\tilde{k}_1\dots\tilde{k}_n} \left(m d_{k_1}^\dagger d_{\tilde{k}_1}^\dagger + n c_{k_1}^\dagger c_{\tilde{k}_1}^\dagger\right) c_{k_2}^\dagger \dots c_{k_m}^\dagger d_{\tilde{k}_2}^\dagger \dots d_{\tilde{k}_n}^\dagger |0\rangle. \tag{A2}$$

where we used the symmetry of $A_{k_1\dots k_m}$ and $B_{k_1\dots k_n}$ under permutations of k's. The expressions $|\langle\psi_\varphi|\dot{\psi}_\varphi\rangle|$ and $\langle\dot{\psi}_\varphi|\dot{\psi}_\varphi\rangle$, which determine the QFI, can be evaluated by using the commutation relations $[c_p, d_k^\dagger] = [d_p, c_k^\dagger] = 0$ and $[c_p, c_k^\dagger] = [d_p, d_k^\dagger] = 2\pi\delta(p-k)$. It is clear that

$$|\langle\psi_\varphi|\dot{\psi}_\varphi\rangle| = 0 \tag{A3}$$

as $|\psi_\varphi\rangle$ and $|\dot{\psi}_\varphi\rangle$ contain a different number of c's and d's. To compute $\langle\dot{\psi}_\varphi|\dot{\psi}_\varphi\rangle$, we use the symmetry of $A_{k_1\dots k_m}$ and $B_{k_1\dots k_n}$, which allows us to take one representative of each of the c_k's or $d_{\tilde{k}}$'s and multiply by the number of times it appears. One has to evaluate an integral over correlation functions $f(X)$ over the k's and $\tilde{k}$'s, for which we introduce the shorthand notation

$$\int dX\, f(X) \equiv \int\!\dots\!\int \frac{\prod_{i,j}^{m,n} dk_i d\tilde{k}_j dp_i d\tilde{p}_j}{(2\pi)^{2(m+n)} m!^2 n!^2} A^*_{p_1\dots p_m} B^*_{\tilde{p}_1\dots\tilde{p}_n} A_{k_1\dots k_m} B_{\tilde{k}_1\dots\tilde{k}_n} f(X). \tag{A4}$$

Then we can write

$$\begin{aligned}
\langle\dot{\psi}_\varphi|\dot{\psi}_\varphi\rangle &= \frac{1}{4}\int dX\, \langle 0| d_{\tilde{p}_n}\dots d_{\tilde{p}_2} c_{p_m}\dots c_{p_2} \left(m d_{p_1} d_{\tilde{p}_1} + n c_{\tilde{p}_1} c_{\tilde{p}_1}\right)\left(m d_{k_1}^\dagger d_{\tilde{k}_1}^\dagger + n c_{k_1}^\dagger c_{\tilde{k}_1}^\dagger\right) c_{k_2}^\dagger \dots c_{k_m}^\dagger d_{\tilde{k}_2}^\dagger \dots d_{\tilde{k}_n}^\dagger |0\rangle \\
&= \frac{1}{4}\int dX\, m^2 \Big(\left[d_{p_1}, d_{k_1}^\dagger\right](m-1)\left[c_{p_2}, c_{k_2}^\dagger\right] n \left[d_{\tilde{p}_1}, d_{\tilde{k}_1}^\dagger\right] + n\left[d_{p_1}, d_{\tilde{k}_1}^\dagger\right] n \left[d_{\tilde{p}_1}, d_{k_1}^\dagger\right](m-1)\left[c_{p_2}, c_{k_2}^\dagger\right]\Big) \\
&\quad \times (m-2)! \prod_{i=3}^{m}\left[c_{p_i}, c_{k_i}^\dagger\right](n-1)! \prod_{j=2}^{n}\left[d_{\tilde{p}_j}, d_{\tilde{k}_j}^\dagger\right] + m \leftrightarrow n
\end{aligned}$$

$$= \frac{1}{4}\int dX\, m!n! \prod_{i=2}^{m} 2\pi\delta(p_i - k_i) \prod_{j=2}^{n} 2\pi\delta(\tilde{p}_j - \tilde{k}_j)[(m+n)(2\pi)^2\delta(p_1 - k_1)\delta(\tilde{p}_1 - \tilde{k}_1)$$
$$+ 2nm(2\pi)^2\delta(p_1 - \tilde{k}_1)\delta(\tilde{p}_1 - k_1)]$$
$$= \frac{1}{4}\big((m+n)I_{AB}^{(0)} + 2mnI_{AB}^{(1)}\big), \tag{A5}$$

where the $I_{AB}^{(0)}$ and $I_{AB}^{(1)}$ read

$$I_{AB}^{(0)} = \int\cdots\int \frac{\prod_{i,j=1,1}^{m,n} dk_i d\tilde{k}_j}{(2\pi)^{m+n} m!n!} \left|A_{k_1,\ldots,k_m}\right|^2 \left|B_{\tilde{k}_1,\ldots,\tilde{k}_m}\right|^2 = 1, \tag{A6a}$$

$$I_{AB}^{(1)} = \int\cdots\int \frac{\prod_{i,j=1,1}^{m,n} dk_i d\tilde{k}_j}{(2\pi)^{m+n} m!n!} A^*_{k_1,\ldots,k_m} B^*_{\tilde{k}_1,\ldots,\tilde{k}_n} A_{\tilde{k}_1,k_2,\ldots,k_m} B_{k_1,\tilde{k}_2,\ldots,\tilde{k}_n}, \tag{A6b}$$

where in $I_{AB}^{(1)}$ the two indices k_1 and $\tilde{k}_1$ have been exchanged in one of the coefficients. The QFI is then given by

$$F_Q[\psi_\varphi] = 4(\langle\dot{\psi}_\varphi|\dot{\psi}_\varphi\rangle - |\langle\psi_\varphi|\dot{\psi}_\varphi\rangle|^2) = 2mnI_{AB}^{(1)} + m + n.$$

This provides the desired result.

Finally, we note that this result can be easily generalized to states of the form

$$\left|\phi_A^{(m)}\right\rangle = \int\cdots\int \frac{dk_1\ldots dk_m}{(2\pi)^m m!} A_{k_1\ldots k_m} a^\dagger_{k_1}\ldots a^\dagger_{k_m}|0\rangle, \quad |\phi_B\rangle = \sum_n c_n \int\cdots\int \frac{d\tilde{k}_1\ldots d\tilde{k}_n}{(2\pi)^n n!} B^{(n)}_{\tilde{k}_1\ldots\tilde{k}_n} b^\dagger_{\tilde{k}_1}\ldots b^\dagger_{\tilde{k}_n}|0\rangle.$$

That is, when an arbitrary pure state with m photons enters one arm, and an arbitrary pure state enters into the other. By noting that states with a different total photon number do not mix, we can use our previous derivation to arrive at the following QFI of $|\psi'_\varphi\rangle = U_\varphi U_{\rm BS}|\phi_A^{(m)}\rangle \otimes |\phi_B\rangle$:

$$F_Q[\psi'_\varphi] = 2m\sum_n \left(|c_n|^2 n I_{AB}^{(1),n}\right) + m + \langle n\rangle, \tag{A7}$$

with $\langle n\rangle = \sum_n |c_n|^2 n$, and

$$I_{AB}^{(1),n} = \int\cdots\int \frac{\prod_{i,j=1,1}^{m,n} dk_i d\tilde{k}_j}{(2\pi)^{m+n} m!n!} A^*_{k_1,\ldots,k_m} B^{(n)*}_{\tilde{k}_1,\ldots,\tilde{k}_n} A_{\tilde{k}_1,k_2,\ldots,k_m} B^{(n)}_{k_1,\tilde{k}_2,\ldots,\tilde{k}_n}. \tag{A8}$$

This result extends one of the results of Ref. [43] on Fock states to arbitrary photonic states of a fixed photon number. We also note that this result holds for pure states, leaving the extension to mixed states as an interesting challenge for the future.

2. Parity measurement

We now show that a parity measurement after the second beam splitter transformation of the MZI locally resolves the phase at the Heisenberg limit when $n = m = N/2$, which is the case of main interest. Strictly speaking, this is achieved in the limit $\varphi \to 0$, but one can always add phase shifters during the estimation processing so that this does not rest generality [1,4].

The measurement operator can be written as $O = U_{\rm BS}^\dagger(-1)^{\int \frac{dk}{2\pi} a_k^\dagger a_k} U_{\rm BS}$, where the beam splitter transformation is generated by $U_{\rm BS} = \exp[\int \frac{dk}{2\pi} i(a_k^\dagger b_k - b_k^\dagger a_k)\pi/4]$, such that

$$O = \prod_k e^{-(a_k^\dagger b_k - b_k^\dagger a_k)\pi/4} e^{i\pi a_k^\dagger a_k} e^{(a_k^\dagger b_k - b_k^\dagger a_k)\pi/4} = \prod_k e^{i(a_k^\dagger - b_k^\dagger)(a_k - b_k)\pi/2}. \tag{A9}$$

We used the transformation $U_{\rm BS}^\dagger a_k^\dagger U_{\rm BS} = \frac{1}{\sqrt{2}}(a_k^\dagger - b_k^\dagger)$. Because $O^2 = 1$, the phase variance around $\varphi \approx 0$ is

$$\Delta\varphi^2 = \lim_{\varphi\to 0} \frac{\langle\Delta O^2\rangle}{(\partial_\varphi\langle O\rangle)^2} = \lim_{\varphi\to 0} \frac{1 - \langle O\rangle^2}{(\partial_\varphi\langle O\rangle)^2} \tag{A10}$$

and only depends on the expectation value $\langle O\rangle = \langle\psi_\varphi|O|\psi_\varphi\rangle$.

This expectation value can be evaluated by using the transformations $O(a^\dagger \pm b^\dagger)O^\dagger = \pm(a^\dagger \pm b^\dagger)$, and therefore $Oc_k^\dagger(\varphi)O^\dagger = c_k^\dagger(-\varphi)$ and $Od_k^\dagger(\varphi)O^\dagger = -d_k^\dagger(-\varphi)$. The expectation value

$$\langle O\rangle = \int\cdots\int \frac{\prod_{i,j}^{m,m} dk_i d\tilde{k}_j dp_i d\tilde{p}_j}{(2\pi)^{4m} m!^4} A^*_{k_1\cdots k_m} B^*_{\tilde{k}_1\cdots\tilde{k}_m} A_{p_1\cdots p_m} B_{\tilde{p}_1\cdots\tilde{p}_m} (-1)^m \langle 0|c_{k_1}(\varphi)\cdots c_{k_m}(\varphi) d_{\tilde{k}_1}(\varphi)\cdots d_{\tilde{k}_m}(\varphi)$$
$$\times c^\dagger_{p_1}(-\varphi)\cdots c^\dagger_{p_m}(-\varphi) d^\dagger_{\tilde{p}_1}(-\varphi)\cdot d^\dagger_{\tilde{p}_m}(-\varphi)|0\rangle$$

can then be further evaluated by using the commutation relations

$$[c_p(\varphi), c_k^\dagger(-\varphi)] = [d_p(\varphi), d_k^\dagger(-\varphi)] = 2\pi\delta(p-q)\cos\varphi, \tag{A11a}$$

$$[c_p(\varphi), d_k^\dagger(-\varphi)] = [d_p(\varphi), c_k^\dagger(-\varphi)] = 2\pi\delta(p-q)i\,\sin\varphi. \tag{A11b}$$

Because the commutators between c_k and d_k do not vanish, all indices can become mixed and the expectation value yields

$$\langle O\rangle = \sum_{l=0}^{m}(-1)^l \sin^{2l}(\varphi)\cos^{2(m-l)}(\varphi)\binom{m}{l}^2 I_m^{(l)}, \tag{A12}$$

where the integrals $I_m^{(l)}$ are the natural extension of (A6), i.e., in $I_m^{(l)}$ l indices are exchanged in the integral. We note that $I_j^{(l)} = I_{m-j}^{(l)}$, such that one can reduce the number of calculations if they are necessary.

By observing that $\partial_\varphi\langle O\rangle|_{\varphi=0} = 0$ and $\langle O\rangle_{\varphi=0} = I_m^{(0)} = 1$, the variance of the measured phase can be calculated from the second derivative,

$$\Delta\varphi^2 = \lim_{\varphi\to 0}\frac{1-\langle O\rangle^2}{(\partial_\varphi\langle O\rangle)^2} = \lim_{\varphi\to 0}\frac{-2\langle O\rangle\partial_\varphi\langle O\rangle}{2\partial_\varphi\langle O\rangle\partial_\varphi^2\langle O\rangle} = \left(-\partial_\varphi^2\langle O\rangle\big|_0\right)^{-1}. \tag{A13}$$

The second derivative around $\varphi\approx 0$ only contains the first two terms, for which the sine terms vanish after the derivative, i.e., $-\partial_\varphi^2\langle O\rangle|_0 = 2m(mI_m^{(1)} + I_m^{(0)})$. Therefore, we reach the QCRB locally around $\varphi\approx 0$,

$$\Delta\varphi^2|_{\varphi\approx 0} = \frac{1}{F_Q\left[\psi_\varphi^{AB}\right]}. \tag{A14}$$

We note that for single-mode states $I_N^{(l)} = 1$, which leads to the result derived in Ref. [44]. In that case the expectation value $\langle O\rangle = P_m[\cos 2\varphi]$ can be expressed in terms of Legendre polynomials P_m. In that case, the second derivative $-\partial_\varphi^2\langle O\rangle|_0 = 4P_m'[1]$ is calculated with the help of the well-known result $P_m'[1] = m(m+1)/2$.

3. Transforming the bidirectional wave packet into a unidirectional one

Let us finally give an example on how to merge the bidirectional wave packet into a unidirectional one with the same metrological properties. The wave packet emitted from each atomic ensemble reads

$$\left|\phi_A^{(N)}\right\rangle = \int_{-\infty}^{\infty}\cdots\int_{-\infty}^{\infty}\frac{dk_1\ldots dk_N}{(2\pi)^N N!}A_{\{k\}}a_{k_1}^\dagger\ldots a_{k_N}^\dagger|0\rangle. \tag{A15}$$

where the k_i integrals run from $(-\infty,\infty)$. This means that the wave packet is actually emitted in both left and right directions. It is possible however to join the left and right emission into a common wave packet by joining both ends of the waveguide through a 50:50 beam splitter transformation. To make it more explicit, we can define r_k/l_k for the a_k modes propagating to the right or left ($k \gtrless 0$), and rewrite the integral with integration ranges from $(0,\infty)$:

$$\left|\phi_A^{(N)}\right\rangle = \int_0^{\infty}\cdots\int_0^{\infty}\frac{dk_1\ldots dk_N}{(2\pi)^N N!}A_{\{k\}}\left[r_{k_1}^\dagger\ldots r_{k_{N-1}}^\dagger r_{k_N}^\dagger + r_{k_1}^\dagger\ldots r_{k_{N-1}}^\dagger l_{k_N}^\dagger + \cdots + l_{k_1}^\dagger\ldots l_{k_{N-1}}^\dagger l_{k_N}^\dagger\right]|0\rangle. \tag{A16}$$

The $A_{\{k\}}$ factorizes out from the sum because it has the symmetry $k_i\to -k_i$ since $\omega(k)\propto|k|$. Notice that now the sum can also be written as a product:

$$\left|\phi_A^{(N)}\right\rangle = \int_0^{\infty}\cdots\int_0^{\infty}\frac{dk_1\ldots dk_N}{(2\pi)^N N!}A_{\{k\}}\left[\prod_{i=1}^{N}(l_{k_i}^\dagger + r_{k_i}^\dagger)\right]|0\rangle. \tag{A17}$$

If the l/r modes are used as inputs of a beam splitter such that the modes transform at the output ports C/D as $c_{k_i}^\dagger = (r_{k_i}^\dagger + l_{k_i}^\dagger)/\sqrt{2}$ and $d_{k_i}^\dagger = (-r_{k_i}^\dagger + l_{k_i}^\dagger)/\sqrt{2}$, then

$$\left|\phi_C^{(N)}\right\rangle = \int_0^{\infty}\cdots\int_0^{\infty}\frac{dk_1\ldots dk_N}{(2\pi)^N N!}2^{N/2}A_{\{k\}}c_{k_i}^\dagger|0\rangle. \tag{A18}$$

Since this state shares the same modal function, $A_{\{k\}}$, as the original one the metrological properties can be shown to be the same as the ones calculated in the main manuscript.

4. Derivation of recurrence relation

We now focus on the evaluation of the integral expression $I_{AB}^{(1)}$ in the case of the same multimode input states, that is, for $m=n=N/2$ and $A_{\{k\}} = B_{\{k\}}$. Since only the integral $I_{AB}^{(1)}$ is relevant for the discussion, from now on, and in the main manuscript we drop the superindex: $I_{AB}^{(1)}\equiv I_{AB}$. If the input state is a product state, that is, if $A_{\{k\}} = \frac{1}{\sqrt{m!}}A_{k_1}A_{k_2}\cdot A_{k_m}$ factorizes, the $I_{2m}\equiv I_{AA}$ can be straightforwardly integrated in each k_i and $\tilde{k}_i$ separately. This calculation yields $I_{2m}=1$, so that the single mode result of $F_Q[\psi_\varphi^{\text{Fock}}] = N(N+2)/2$ is recovered.

On the other hand, the coefficient of the photonic state emitted from a chain of quantum emitters along a waveguide does not factorize in this way, such that the evaluation of I_{2m} requires additional effort. Because the multimode coefficients originate from the exponential decay of the emitters,

$$A_{\{k\}} = (-i)^m\int_0^{\infty}\prod_i dt_i\, e^{i\sum_i k_i t_i}\mathcal{T}\langle 0|O_{t_1}O_{t_2}\cdots O_{t_m}|\psi_m\rangle, \tag{A19}$$

where $O_t\equiv O(t) = \sqrt{\Gamma_{1d}}e^{iH_{\text{eff}}t}S_{ge}e^{-iH_{\text{eff}}t}$ with the effective Hamiltonian $H_{\text{eff}} = (\Delta - i\frac{\Gamma^*}{2})S_{ee} - i\frac{\Gamma_{1d}}{2}S_{eg}S_{ge}$ acting on the symmetric Dicke states $|\psi_m\rangle = \frac{1}{m!}\binom{N}{m}^{-1/2}S_{eg}^m|0\rangle$. The action of the time ordering operator $\mathcal{T}$ on commuting operators is defined as $\mathcal{T}O_{t_1}O_{t_2} = \theta(t_1-t_2)O_{t_1}O_{t_2} + \theta(t_2-t_1)O_{t_2}O_{t_1}$. Using this expression for the coefficients $A_{\{k\}}$ the integrals

in momentum space can be transformed to integrals in time,

$$I_{2m} = \frac{1}{m!^2}\int_0^\infty \prod_{i,j} dt_i ds_j \mathcal{T}\langle 0|O_{t_1}O_{t_2}\cdots O_{t_m}|\psi_m\rangle^*\langle 0|O_{s_1}O_{s_2}\cdots O_{t_m}|\psi_m\rangle^*\langle 0|O_{s_1}O_{t_2}\cdots O_{t_m}|\psi_m\rangle\langle 0|O_{t_1}O_{s_2}\cdots O_{t_m}|\psi_m\rangle. \quad \text{(A20)}$$

Notice that in the correlation functions one index is exchanged, in analogy with the expressions in momentum space, and that the integral is symmetric with respect to the remaining t_i/s_j indices.

The integral can be evaluated recursively by picking a time ordering and integrating over the latest time $\tau \geqslant \max_{\neq\tau}\{t_i, s_i\} \equiv T$, and repeating this step on the next integral. The exponential decay then gives rise to the simple form of $\int_T^\infty e^{-c\tau} = \frac{1}{c}e^{-cT}$ if $\mathrm{Re}(c) > 0$. Using these results, one can define three structurally different integrals, depending on whether one has already integrated over one or both of the special (i.e., exchanged) indices t_1 or s_1,

$$F_{ij}^{(2)} = \int \prod_{i',j'} dt_{i'} ds_{j'} \mathcal{T}\, e^{-c_{ij}^{(2)}\max\{t_{i'},s_{j'}\}}\langle\psi_{m-1-i}|O_{t_1}O_{t_2}\cdots O_{t_{i+1}}|\psi_m\rangle^*\langle\psi_{m-1-j}|O_{s_1}O_{s_2}\cdots O_{s_{j+1}}|\psi_m\rangle^*\langle\psi_{m-1-i}|O_{s_1}O_{t_2}\cdots O_{t_{i+1}}|\psi_m\rangle$$
$$\times\langle\psi_{m-1-j}|O_{t_1}O_{s_2}\cdots O_{s_{j+1}}|\psi_m\rangle, \quad \text{(A21a)}$$

$$F_{ij}^{(1)} = \int \prod_{i',j'} dt_{i'} ds_{j'} \mathcal{T}\, e^{-c_{ij}^{(1)}\max\{t_{i'},s_{j'}\}}\langle\psi_{m-1-i}|O_{t_1}O_{t_2}\cdots O_{t_{i+1}}|\psi_m\rangle^*\langle\psi_{m-j}|O_{s_2}\cdots O_{s_{j+1}}|\psi_m\rangle^*\langle\psi_{m-i}|O_{t_2}\cdots O_{t_{i+1}}|\psi_m\rangle$$
$$\times\langle\psi_{m-1-j}|O_{t_1}O_{s_2}\cdots O_{s_{j+1}}|\psi_m\rangle, \quad \text{(A21b)}$$

$$F_{ij}^{(0)} = \int \prod_{i',j'} dt_{i'} ds_{j'} \mathcal{T}\, e^{-c_{ij}^{(0)}\max\{t_{i'},s_{j'}\}}\langle\psi_{m-i}|O_{t_2}\cdots O_{t_{i+1}}|\psi_m\rangle^*\langle\psi_{m-j}|O_{s_2}\cdots O_{s_{j+1}}|\psi_m\rangle^*\langle\psi_{m-i}|O_{t_2}\cdots O_{t_{i+1}}|\psi_m\rangle$$
$$\times\langle\psi_{m-j}|O_{s_2}\cdots O_{s_{j+1}}|\psi_m\rangle. \quad \text{(A21c)}$$

The integrals only run over the remaining time variables $\{t_{i'}\}$ and $\{s_{j'}\}$ and we have introduced the exponents $c_{ij}^{(2)} = \gamma_{m-1-i} + \gamma_{m-1-j}$, $c_{ij}^{(0)} = \gamma_{m-i} + \gamma_{m-j}$, and $c_{ij}^{(1)} = (c_{ij}^{(2)} + c_{ij}^{(0)})/2$. The decay rates are given by $\gamma_j = j(N-j+1)\Gamma_{1\mathrm{d}}$ defined through $\Gamma_{1\mathrm{d}}S_{eg}S_{ge}|\psi_j\rangle = \gamma_j|\psi_j\rangle$. Note that these integrals always converge because $c_{ij}^{(2/1/0)} > 0$.

By integrating over the latest time, one can remove one operator O_{t_i} or O_{s_j} from the above expressions until one ends up with $F_{00}^{(0)} = 1$. This motivates the fact that the integral

$$I_{2m} = \frac{1}{m!^2}F_{m-1,m-1}^{(2)} \quad \text{(A22)}$$

can be evaluated by a recurrence relation (see also Fig. 3). Let us understand the structure of the recurrence relation on the example of $F_{ij}^{(2)}$. If the largest time is one with a regular index $t_2, \ldots, t_{i+1}$ (for which there are i possibilities), we use the fact that

$$\langle\psi_{m-1-i}|O_{t_{i+1}} = \sqrt{\gamma_{m-i}}e^{-(\gamma_{m-i}-\gamma_{m-i-1})t_{i+1}/2}\langle\psi_{m-1-i}|. \quad \text{(A23)}$$

This term appears twice such that the integral gives a prefactor $\frac{\gamma_{m-i}}{c_{ij}^{(2)}+(\gamma_{m-i}-\gamma_{m-i-1})} = \frac{\gamma_{m-i}}{c_{i-1,j}^{(2)}}$. The remaining integral is then of the form $F_{i-1,j}^{(2)}$. The same holds if the largest time is one of $s_2, \ldots, s_{j+1}$. If the largest time is s_1 (or equivalently t_1), then after the integration over this variable, the remaining integral is of the form $F_{ij}^{(1)}$. By carefully calculating all these steps, we find the recurrence relation:

$$F_{ij}^{(2)} = i\frac{\gamma_{m-i}}{c_{i-1,j}^{(2)}}F_{i-1,j}^{(2)} + j\frac{\gamma_{m-j}}{c_{i,j-1}^{(2)}}F_{i,j-1}^{(2)} + 2\frac{\sqrt{\gamma_{m-i}\gamma_{m-j}}}{c_{i,j}^{(1)}}F_{i,j}^{(1)}, \quad \text{(A24a)}$$

$$F_{ij}^{(1)} = i\frac{\sqrt{\gamma_{m-i}\gamma_{m-i+1}}}{c_{i-1,j}^{(1)}}F_{i-1,j}^{(1)} + j\frac{\sqrt{\gamma_{m-j}\gamma_{m-j+1}}}{c_{i,j-1}^{(1)}}F_{i,j-1}^{(1)} + \frac{\sqrt{\gamma_{m-i}\gamma_{m-j}}}{c_{i,j}^{(0)}}F_{i,j}^{(0)}, \quad \text{(A24b)}$$

$$F_{ij}^{(0)} = i\frac{\gamma_{m-i+1}}{c_{i-1,j}^{(0)}}F_{i-1,j}^{(0)} + j\frac{\gamma_{m-j+1}}{c_{i,j-1}^{(0)}}F_{i,j-1}^{(0)}, \quad \text{(A24c)}$$

$$F_{00}^{(0)} = 1. \quad \text{(A24d)}$$

The trick to evaluating this recurrence relation efficiently is to group elements of the same excitation subspace $0 \leqslant k \leqslant 2m$ as in Fig. 3. Elements of this subspace are, for example, $F_{ij}^{(2)}$ satisfying $i+j+2 = k$ and $0 \leqslant i, j \leqslant m-1$. By applying one recursive step starting from $k = 0$, in which only $F_{00}^{(0)} = 1$ lies, one moves to a subspace with one excitation more $k \to k+1$ until $k = 2m$ is reached. This subspace only contains the desired term $F_{m-1,m-1}^{(2)}$. For better numerical results it is also recommendable to remove the factors of i and j by substituting $F_{ij}^{(n)} = i!\,j!\,\tilde{F}_{ij}^{(n)}$.

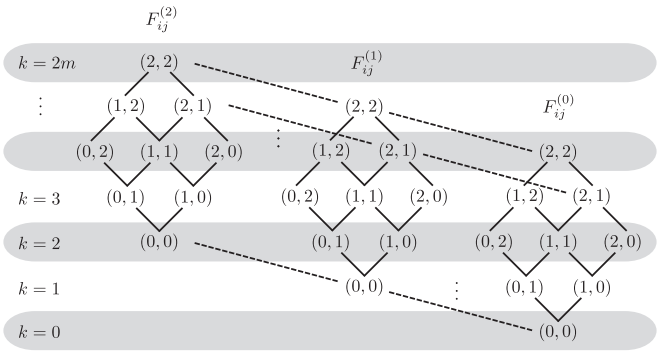

FIG. 3. Recurrence relation of $F_{ij}^{(2/1/0)}$ to calculate I_m can be represented pictorially; here on the example of $m = 3$. The solid lines represent the terms of the recurrence relation in between every group $F^{(n)} \to F^{(n)}$, whereas the dashed lines correspond to the terms $F^{(2)} \to F^{(1)}$ and $F^{(1)} \to F^{(0)}$. By grouping the elements in terms of the number of excitations, or equivalently the number of remaining time integrals, one can evaluate the recurrence relation efficiently.

5. Robustness to errors

In this section, we estimate how the different error sources affect our protocol, deriving the conditions under which they can be neglected. In particular, we study the impact of (i) free-space spontaneous emission, (ii) finite propagation length of the modes, (iii) retardation effects due to finite group velocity, (iv) different coupling to the waveguide of the two emitter ensembles, (v) time delay between the different wave packets, and (vi) photon loss in the interferometer.

a. Impact of emission into free space

One of the greatest sources of decoherence in state-of-the-art waveguide QED systems is the possibility of emitting to other modes different from the relevant waveguide one. We embed all these processes into a single decay rate, Γ^*, and describe through an individual Lindblad decay terms as follows:

$$\mathcal{L}_*[\rho] = \frac{\Gamma^*}{2}\sum_{n=1}^{N}\left(2\sigma_{ge}^n\rho\sigma_{eg}^n - \sigma_{ee}^n\rho - \rho\sigma_{ee}^n\right). \tag{A25}$$

With this extra term, the effective non-Hermitian Hamiltonian governing the atomic state evolution contains now two contributions: the collective and individual decay terms, which read

$$H_{\text{eff}} = -i\left(\frac{\Gamma_{1\text{d}}}{2}S_{eg}S_{ge} + \frac{\Gamma^*}{2}\sum_n \sigma_{ee}^n\right), \tag{A26}$$

as well as the quantum jumps evolution:

$$J[\rho] = J_{1\text{d}}[\rho] + J_*[\rho], \tag{A27}$$

$$J_{1\text{d}}[\rho] = \Gamma_{1\text{d}}S_{ge}\rho S_{eg}, \tag{A28}$$

$$J_*[\rho] = \Gamma^*\sum_n \sigma_{ge}^n\rho\sigma_{eg}^n. \tag{A29}$$

The formal evolution of $\rho(t)$ can be formally integrated as a sum of different contributions: $\rho(t) = \sum_j \rho_j(t)$ depending on the number of quantum jumps, denoted by j, that has occurred during the evolution. In particular, the different $\rho_j(t)$ can be formally computed as

$$\rho_0(t) = S(t, t_0)\rho(t_0), \tag{A30}$$

$$\rho_{j\geqslant 1}(t) = \int_0^t dt_1 S(t, t_1)J[\rho_{j-1}(t_1)], \tag{A31}$$

where we have defined the following operator: $S(t_2, t_1)[\rho] = e^{-iH_{\text{eff}}t}\rho\, e^{iH_{\text{eff}}^\dagger t}$, which gives the evolution under the non-Hermitian Hamiltonian. Since we assume an initial state $|\Psi(0)\rangle = |e\rangle^{\otimes N}$ and we are only interested in the probability of decaying to $|g\rangle^{\otimes N}$ only through collective quantum jumps (denoted as p in the main text), we restrict our attention to the dynamics of the collective atomic states with m excitations, that is, $|m\rangle \propto S_{ge}^{N-m}|\Psi(0)\rangle$, that we denote as

$$P_m(t) = \langle m|\rho(t)|m\rangle. \tag{A32}$$

Using this notation $P_0(t \to \infty) \equiv p$. Since only collective quantum jumps participate in the evolution of $P_m(t)$, their dynamics can be calculated straightforwardly from Eqs. (A30) and (A31). First, note that the non-Hermitian Hamiltonian only connects states with the same number of excitations, such that

$$S(t_2, t_1)[|m\rangle\langle m|] = |m\rangle\langle m|e^{-[\Gamma_{1\text{d}}m(N-m+1)+m\Gamma^*](t_2-t_1)}. \tag{A33}$$

For example, the evolution of the higher excited state is simply given by

$$P_N(t) = e^{-(\Gamma_{1\text{d}}+\Gamma^*)Nt}. \tag{A34}$$

From here, the evolution of the $p_{m<N}(t)$ can be calculated recursively using Eq. (A31):

$$P_m(t) = m(N-m++1)\Gamma_{1\text{d}} \times \int_0^t dt_1 e^{-[(m-1)(N-m+2)\Gamma_{1\text{d}}+(m-1)\Gamma^*](t-t_1)}P_{m+1}(t). \tag{A35}$$

Using these formulas one can calculate the dynamics of $P_m(t)$ for all m and the set of parameters N, $\Gamma_{1\text{d}}$, and Γ^*. To gain intuition from the decay process, we start calculating $P_m(t)$ for a situation with $\Gamma^* = 0$, that we show in different colors in Fig. 4(a) for a situation with $N = 20$ QEs. We start observing a collective decay from the highly excited state (in red) $m = N = 20$, as the lower excited level starts building up population until it gets accumulated in $m = 0$. From this figure, it may look as if the transient time through the higher excited states was faster than in the smaller ones. However, by looking into the averaged time population,

$$\bar{P}_m = \int_0^\infty dt\, P_m(t), \tag{A36}$$

which we plot in the inset of the figure, we observe that in fact the average time spent in each of the levels distribute symmetrically around $m = N/2 + 1$. Thus, when considering $\Gamma^* \neq 0$, the main source of errors will come from the upper part of the ladder $m \approx N$, since the decay rate into free space is proportional to the number of excitations $\sim m\Gamma^*$.

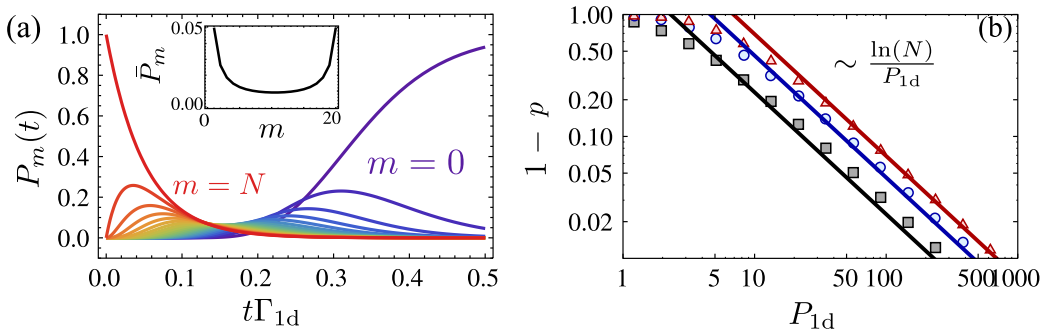

FIG. 4. (a) $P_m(t)$ for a situation with $N = 20$ and P_{1d} for different m ranging from $m = N = 20$ (red, left) to $m = 0$ (purple, right). Inset: integrated population $\bar{P}_m = \int_0^\infty P_m(t)dt$ with the parameters. (b) $1 - P_0(t \to \infty)$ $[1 - p]$ as a function of P_{1d} for $N = 10$ (black squares), $N = 100$ (blue spheres), and $N = 1000$ (red triangles).

In Fig. 4(b) we show the effect of $\Gamma^* \neq 0$ on p, which is the relevant parameter to estimate the lower bound of the QFI given in the main text. In particular, we plot the scaling of $1 - p$ as a function of $P_{1d} = \frac{\Gamma_{1d}}{\Gamma^*}$ for several N's as depicted in the legend. We observe that the exact calculation of $1 - p$ obtains the same scaling, $\ln(N)/P_{1d}$, as we show in the main text with a simplified description of the losses.

This error scaling can also be obtained by estimating the time scale of the superradiant decay as the sum of the different decay time scales of $P_m(t)$, which leads to

$$\tau_{SR} \approx \sum_{j=1}^{N} \frac{1}{\Gamma_{1d} j(N - j + 1)} \sim \frac{\ln(N)}{N\Gamma_{1d}}. \tag{A37}$$

With this time scale, one can easily upper bound the error of $1 - p$ by multiplying this time scale by the maximum error rate, $N\Gamma^*$, from the higher excited state. This results into an upper bound

$$1 - p \leqslant N\Gamma^* \tau_{SR} \approx \frac{\ln(N)}{P_{1d}}, \tag{A38}$$

which has the same scaling as the one observed in the numerical simulations.

b. Finite lifetime of waveguide modes

Another possible source of decoherence is the finite lifetime of the photonic waveguide modes, which appears due to absorption or imperfections in the material which leads to scattering into other modes. These photonic losses affect the metrological properties during and after the N-photon emission. The effect of the losses after the wave packet has been emitted can be considered as noise within the interferometric process, which has been well studied in the literature [4], leading to a loss of Heisenberg scaling for large N. Since this is a common limitation of all metrological protocols, we focus on the effect of photon losses during the emission of the N-photon wave packet.

During the emission of the waveguide, the finite lifetime of waveguide modes induce a finite propagation of waveguide modes, L_{prop}, which spoils the collective behavior of the emitter interactions as follows:

$$\Gamma_{m,n} = \Gamma_{1d} e^{-|x_n - x_m|/L_{prop}}. \tag{A39}$$

To be able to neglect this correction, the propagation length of the modes has to be much larger than the system size, that is, $L_{prop} \gg N\lambda_a$, where we have assumed a separation between atoms of the order of λ_a, required to have the perfect collective behavior. The propagation length of the modes is approximately given by [35]

$$\frac{L_{prop}}{\lambda_a} \approx \frac{Q}{2n_g}, \tag{A40}$$

where Q is the experimental quality factor of the waveguide modes, whereas n_g is the so-called group index, which measures the reduction of the speed of light within the waveguide. Thus the inequality that must be satisfied is that

$$\frac{Q}{2n_g} \gg N. \tag{A41}$$

State-of-the-art numbers with SiN waveguides [26] are $Q \approx 10^6$ and $n_g \approx 10$, which gives $L_{prop}/\lambda_a \approx 5 \times 10^4$. Since this size is even larger than typical waveguide lengths, this correction will be typically small.

c. Retardation effects: Validity of the Markov approximation

All the calculations shown in this manuscript, including the one of the spectral shape of the wave packet, $A_{\{q\}}$, are performed by using a Born-Markov master equation describing the atomic dynamics as written in the main text. The underlying assumption of this equation is that the bath time scales are faster than the emitter ones. In particular, the emergence of superradiant behavior as predicted by Dicke superradiance requires that the propagation time of the photons between all the emitters is faster than the fastest emitter time scale. The maximum propagation time for a system with N emitters is given by

$$\tau_{prop} = \frac{N\lambda_a}{v_g}, \tag{A42}$$

where $v_g = c/n_g$ is the group velocity of the photons in the waveguide. The fastest atomic time scale occurs in the middle of the Dicke ladder, where the decay rate scales with $\sim\Gamma_{1d}N^2/4$. Thus the condition that must be satisfied is that

$$\tau_{prop} \ll \frac{4}{\Gamma_{1d}N^2} \to N^3 \ll \frac{4c}{n_g\lambda_a\Gamma_{1d}}. \tag{A43}$$

Using state-of-the-art numbers of $\Gamma_{1d} \sim 2\pi \times 6$ MHz, $n_g \approx 10$, and $\lambda_a = 300$ nm, we find $4c/(n_g \lambda_a \Gamma_{1d}) \sim 10^7$, which implies $N < 200$. Moreover, by making use of a Raman transition, one can decrease Γ_{1d}, while at the same time attenuating Γ^* such that P_{1d} remains fixed.

d. Different Purcell factors between wave packets

Until now we have assumed that the ensembles generating the multimode state $|\phi_A^N\rangle$ are coupled with the same decay rate, Γ_{1d}, to the waveguide modes. Let us now assume they are different, that is, that they are coupled with Γ_{1d} and Γ'_{1d}, respectively. Note that this does not affect the norm of the state, but it does change the integral I_N. This can still be evaluated by a similar recurrence relation as in (A24). The only difference is that in every numerator one has to replace $\gamma_j \to \sqrt{\gamma_j \gamma'_j}$ and in every denominator, that is in every $c_{ij}^{(l)}$, $\gamma_j \to \frac{1}{2}(\gamma_j + \gamma'_j)$. Because $\gamma'_j = \gamma_j \frac{\Gamma'_{1d}}{\Gamma_{1d}}$ every step of the recurrence relation gets an additional factor of $\frac{\sqrt{\Gamma'_{1d}/\Gamma_{1d}}}{\frac{1}{2}(1+\Gamma'_{1d}/\Gamma_{1d})}$. As there are N steps in the recurrence relation, the integral I_N has to be replaced by

$$I_{N,\Delta\Gamma_{1d}} = \left(\frac{2\sqrt{\Gamma_{1d}\Gamma'_{1d}}}{\Gamma_{1d}+\Gamma'_{1d}}\right)^N I_N = I_N\left(1 - \frac{N}{8}\left(\frac{\Delta\Gamma_{1d}}{\Gamma_{1d}}\right)^2 + O\left[\left(\frac{\Delta\Gamma_{1d}}{\Gamma_{1d}}\right)^3\right]\right), \quad \text{(A44)}$$

where $\Delta\Gamma_{1d} = (\Gamma_{1d} - \Gamma'_{1d})$.

e. Time delay between wave packets

Another deviation from the ideal situation appears if the wave packets emitted from the first or second ensemble do not arrive simultaneously to the beam splitter. This can occur if either the collective π pulse exciting the ensembles is not perfectly simultaneous or the traveling path between the two wave packets is not exactly matched. In both cases, they will give rise to a time delay, τ, between the two wave packets. This time delay enters in the integral I_N as follows:

$$I_{N,\tau} = \int\cdots\int \frac{\prod_{i=1}^n dk_i d\tilde{k}_i}{(2\pi)^{2n} n!n!} A^*_{k_1,\ldots,k_n} A^*_{\tilde{k}_1,\ldots,\tilde{k}_n} A_{\tilde{k}_1,k_2,\ldots,k_n} A_{k_1,\tilde{k}_2,\ldots,\tilde{k}_n} e^{-i\tau(k_1-\tilde{k}_1)}, \quad \text{(A45)}$$

where $n = N/2$ and τ is the delay between the wave fronts. By transforming this integral in momentum space to an integral in time space, we find that it is equivalent to

$$I_{N,\tau} = \frac{1}{n!^2}\int_0^\infty \prod_i dt_i \int_{-\tau}^\infty \prod_j ds_j \theta(t_1-\tau) e^{-\gamma_n \tau} \langle 0|\mathcal{T} O_{t_1} O_{t_2}\cdots O_{t_m}|\psi_n\rangle^* \langle 0|\mathcal{T} O_{s_1} O_{s_2}\cdots O_{t_m}|\psi_n\rangle^* \times \langle 0|\mathcal{T} O_{s_1} O_{t_2}\cdots O_{t_m}|\psi_n\rangle \langle 0|\mathcal{T} O_{t_1} O_{s_2}\cdots O_{t_m}|\psi_n\rangle, \quad \text{(A46)}$$

where $\theta(x)$ is the Heaviside function. One can find a similar recurrence relation, which one can lower bound by noting that $\int_T^\infty dt\, \theta(t-\tau) e^{-ct} \geqslant \theta(T-\tau) \int_T^\infty dt\, e^{-ct}$. This means that the Heaviside function appears in every remaining integral after the integral over t_1 has been performed. The final integral is then either of the form $\int_0^\infty dt\, \theta(t-\tau) e^{-\gamma_n t}$ or $\int_{-\tau}^\infty ds\, \theta(s-\tau) e^{-\gamma_n s}$, which both yield an additional factor of $e^{-\gamma_n \tau}$ in addition to the integral one would have to perform without the time delay. Therefore, the integral $I_{N,\tau}$ is lower bounded by

$$I_{N,\tau} \geqslant e^{-2\gamma_n \tau} I_N = e^{-2\gamma_{N/2}\tau} I_N \approx I_N(1 - N\Gamma_{1d}\tau + O[(N\Gamma_{1d}\tau)^2]). \quad \text{(A47)}$$

One can compare this to the single-mode result, for which one obtains

$$I_{N,\tau} = e^{-\gamma_1 \tau} \approx 1 - N\Gamma_{1d}\tau/2 + O[(N\Gamma_{1d}\tau)^2]. \quad \text{(A48)}$$

f. Photon loss in the interferometer

In this section, we characterize the first-order corrections due to photon loss in one arm of the interferometer. This is described by a beam splitter that mixes the modes b_k with an external mode (e_k) in the vacuum state with a reflection coeffficient $\sqrt{\eta}$. That is,

$$b_k \longrightarrow \sqrt{1-\eta} b_k + \sqrt{\eta} e_k^\dagger. \quad \text{(A49)}$$

We also focus on the case $m = n = N/2$ and for twin states $A = B$. Due to the mixing (A49) the state $|\psi_\varphi\rangle$ changes as

$$|\psi_\varphi\rangle \longrightarrow |\psi_\varphi\rangle^{\text{noise}} = \int\cdots\int \frac{\prod_{i,j=1}^{m,n} dk_i d\tilde{k}_j}{(2\pi)^{2n} n!^2} A_{k_1\ldots k_n} A_{\tilde{k}_1\ldots\tilde{k}_n} \times \prod_j \frac{1}{2}\big(e^{-i\varphi/2} a_{k_j}^\dagger + e^{i\varphi/2}\big(\sqrt{1-\eta} b_{k_j}^\dagger + \sqrt{\eta} e_{k_j}^\dagger\big)\big)\big(-e^{-i\varphi/2} a_{\tilde{k}_j}^\dagger + e^{i\varphi/2}\big(\sqrt{1-\eta} b_{k_j}^\dagger + \sqrt{\eta} e_{k_j}^\dagger\big)\big)|0\rangle. \quad \text{(A50)}$$

After tracing out over the undesired mode e_k $\forall k$ the state can be written as

$$\rho = \text{Tr}_e\big(|\psi_\varphi\rangle^{\text{noise}}\langle\psi_\varphi|^{\text{noise}}\big) = \sum_{j=0}^{N} p_j \sigma^{(j)}, \quad \text{(A51)}$$

where $\sigma^{(j)}$ is a state that has lost j photons into the modes e_k. Because each state has a different photon number, it follows that

$$F_Q[\rho] = \sum_{j=0}^{N} p_j F_Q[\sigma^{(j)}]. \quad \text{(A52)}$$

The computation of $F_Q[\sigma^{(j)}]$ is challenging because the $\sigma^{(j)}$'s with $1 \leqslant j < N$ are mixed states when the state is multimode. The techniques developed here only allow for dealing with pure states, and we leave the development of techniques to compute the QFI of mixed multimode states as an interesting problem for the future. Here, instead, we focus on the regime of small losses and characterize the first-order corrections to the QFI due to photon loss.

We now focus on the limit $\eta \ll 1$, and in what follows we will only keep first-order corrections in η [so that $\approx$ stands for equality up to corrections of order $O(\eta^2)$]. We focus on the state $\sigma^{(0)}$, which is a pure state $\sigma^{(0)} = |\psi_\varphi^{(0)}\rangle\langle\psi_\varphi^{(0)}|$ as no photons have been lost. We have $p_0\sigma^{(0)} = |\tilde{\psi}_\varphi^{(0)}\rangle\langle\tilde{\psi}_\varphi^{(0)}|$ with the non-normalized state

$$\big|\tilde{\psi}_\varphi^{(0)}\big\rangle = \int\cdots\int \frac{\prod_{i,j=1}^{n} dk_i d\tilde{k}_j}{(2\pi)^{2n} n!^2} A_{k_1\ldots k_n} A_{\tilde{k}_1\ldots\tilde{k}_n} \tilde{c}_{k_1}^\dagger \ldots \tilde{c}_{k_n}^\dagger \tilde{d}_{\tilde{k}_1}^\dagger \ldots \tilde{d}_{\tilde{k}_n}^\dagger |0\rangle, \quad \text{(A53)}$$

where we defined

$$\tilde{c}_k^\dagger = \frac{1}{\sqrt{2}}\big(e^{-i\varphi/2} a_{k_j}^\dagger + e^{i\varphi/2}\sqrt{1-\eta} b_{k_j}^\dagger\big) \approx c_{k_j}^\dagger - \frac{\eta e^{i\varphi/2}}{2\sqrt{2}} b_{k_j}^\dagger, \quad \tilde{d}_k^\dagger = \frac{1}{\sqrt{2}}\big(-e^{-i\varphi/2} a_{k_j}^\dagger + e^{i\varphi/2}\sqrt{1-\eta} b_{k_j}^\dagger\big) \approx d_{k_j}^\dagger - \frac{\eta e^{i\varphi/2}}{2\sqrt{2}} b_{k_j}^\dagger. \quad \text{(A54)}$$

Expanding $|\tilde{\psi}_\varphi^{(0)}\rangle$ at first order in η we obtain

$$\begin{aligned}\big|\tilde{\psi}_\varphi^{(0)}\big\rangle &\approx \int\cdots\int \frac{\prod_{i,j=1}^{n} dk_i d\tilde{k}_j}{(2\pi)^{2n} n!^2} A_{k_1\ldots k_n} A_{\tilde{k}_1\ldots\tilde{k}_n} \left(c_{k_1}^\dagger d_{\tilde{k}_1}^\dagger - \frac{n\eta\, e^{i\varphi/2}}{2\sqrt{2}}\big(b_{k_1}^\dagger d_{\tilde{k}_1}^\dagger + c_{k_1}^\dagger b_{\tilde{k}_1}^\dagger\big)\right) c_{k_2}^\dagger \ldots c_{k_n}^\dagger d_{\tilde{k}_2}^\dagger \ldots d_{\tilde{k}_n}^\dagger |0\rangle, \\ &= \int\cdots\int \frac{\prod_{i,j=1}^{n} dk_i d\tilde{k}_j}{(2\pi)^{2n} n!^2} A_{k_1\ldots k_n} A_{\tilde{k}_1\ldots\tilde{k}_n} \left(c_{k_1}^\dagger d_{\tilde{k}_1}^\dagger - \frac{n\eta}{4}\big(2c_{k_1}^\dagger d_{\tilde{k}_1}^\dagger + d_{k_1}^\dagger d_{\tilde{k}_1}^\dagger + c_{\tilde{k}_1}^\dagger c_{k_1}^\dagger\big)\right) c_{k_2}^\dagger \ldots c_{k_n}^\dagger d_{\tilde{k}_2}^\dagger \ldots d_{\tilde{k}_n}^\dagger |0\rangle, \end{aligned} \quad \text{(A55)}$$

where we used the symmetry of $A_{k_1\ldots k_n}$ and $B_{\tilde{k}_1\ldots\tilde{k}_n}$ over permutations. By a similar calculation of the ones performed in the previous sections, and recalling that c_k (d_k) commutes with $d_k^\dagger$ (d_k), one obtains

$$\big\langle\tilde{\psi}_\varphi^{(0)}\big|\tilde{\psi}_\varphi^{(0)}\big\rangle \approx 1 - n\eta. \quad \text{(A56)}$$

Hence we have that

$$p_0 \approx 1 - n\eta \quad \text{(A57)}$$

and $\sigma^{(0)} = |\psi_\varphi^{(0)}\rangle\langle\psi_\varphi^{(0)}|$ with

$$\begin{aligned}\big|\psi_\varphi^{(0)}\big\rangle &\approx \frac{1}{\sqrt{1-n\eta}}\big|\tilde{\psi}_\varphi^{(0)}\big\rangle \approx \left(1 + \frac{n\eta}{2}\right)\big|\tilde{\psi}_\varphi^{(0)}\big\rangle \\ &= \int\cdots\int \frac{\prod_{i,j=1}^{n} dk_i d\tilde{k}_j}{(2\pi)^{2n} n!^2} A_{k_1\ldots k_n} A_{\tilde{k}_1\ldots\tilde{k}_n} \left(c_{k_1}^\dagger d_{\tilde{k}_1}^\dagger - \frac{n\eta}{4}\big(d_{k_1}^\dagger d_{\tilde{k}_1}^\dagger + c_{\tilde{k}_1}^\dagger c_{k_1}^\dagger\big)\right) c_{k_2}^\dagger \ldots c_{k_n}^\dagger d_{\tilde{k}_2}^\dagger \ldots d_{\tilde{k}_n}^\dagger |0\rangle. \end{aligned} \quad \text{(A58)}$$

To compute the corrections to the QFI, consider

$$|\dot{\psi}_\varphi^{(0)}\rangle \approx \int\!\dots\!\int \frac{\prod_{i,j=1}^{n} dk_i d\tilde{k}_j}{\sqrt{1-n\eta}(2\pi)^{2n}n!^2} A_{k_1\dots k_n}A_{\tilde{k}_1\dots\tilde{k}_n}\big(nd_{k_1}^\dagger d_{\tilde{k}_1}^\dagger c_{k_2}^\dagger d_{\tilde{k}_2}^\dagger + nc_{k_1}^\dagger c_{\tilde{k}_1}^\dagger c_{k_2}^\dagger d_{\tilde{k}_2}^\dagger - \frac{n\eta}{4}\big[2c_{k_1}^\dagger d_{\tilde{k}_1}^\dagger c_{k_2}^\dagger d_{\tilde{k}_2}^\dagger + 2nd_{k_1}^\dagger c_{\tilde{k}_1}^\dagger c_{k_2}^\dagger d_{\tilde{k}_2}^\dagger$$
$$+ (n-1)d_{k_1}^\dagger d_{\tilde{k}_1}^\dagger d_{k_2}^\dagger d_{\tilde{k}_2}^\dagger + (n-1)c_{k_1}^\dagger c_{\tilde{k}_1}^\dagger c_{k_2}^\dagger c_{\tilde{k}_2}^\dagger\big]\big)c_{k_3}^\dagger \dots c_{k_n}^\dagger d_{\tilde{k}_3}^\dagger \dots d_{\tilde{k}_n}^\dagger|0\rangle. \tag{A59}$$

Using the shorthand notation

$$\int dX\, f(X) \equiv \int\!\dots\!\int \frac{\prod_{i,j}^{n} dk_i d\tilde{k}_j dp_i d\tilde{p}_j}{(2\pi)^{4n}n!^4} A^*_{p_1\cdots p_n}A^*_{\tilde{p}_1\cdots\tilde{p}_n}A_{k_1\cdots k_n}A_{\tilde{k}_1\cdots\tilde{k}_n} f(X), \tag{A60}$$

we proceed to compute

$$\begin{aligned}\langle\psi_\varphi^{(0)}|\dot{\psi}_\varphi^{(0)}\rangle &\approx \frac{-n\eta}{4}\Bigg(\int dX\,\langle 0|c_{p_1}\cdots c_{p_n}d_{\tilde{p}_1}\cdots d_{\tilde{p}_n}\big(2c_{k_1}^\dagger d_{\tilde{k}_1}^\dagger c_{k_2}^\dagger d_{\tilde{k}_2}^\dagger + 2nd_{k_1}^\dagger c_{\tilde{k}_1}^\dagger c_{k_2}^\dagger d_{\tilde{k}_2}^\dagger\big)c_{k_3}^\dagger\dots c_{k_n}^\dagger d_{\tilde{k}_3}^\dagger\dots d_{\tilde{k}_n}^\dagger|0\rangle \\ &\quad + n\int dX\big[\langle 0|c_{p_1}\cdots c_{p_n}c_{\tilde{p}_1}d_{\tilde{p}_2}\cdots d_{\tilde{p}_n}c_{k_1}^\dagger\dots c_{k_n}^\dagger c_{\tilde{k}_1}^\dagger d_{\tilde{k}_2}^\dagger\dots d_{\tilde{k}_n}^\dagger|0\rangle + c\leftrightarrow d\big]\Bigg) \\ &= \frac{-n\eta}{4}\Bigg(2 + 2nI_{2n} + n\int dX\big[\langle 0|c_{p_1}\cdots c_{p_n}c_{\tilde{p}_1}d_{\tilde{p}_2}\cdots d_{\tilde{p}_n}c_{k_1}^\dagger\dots c_{k_n}^\dagger c_{\tilde{k}_1}^\dagger d_{\tilde{k}_2}^\dagger\dots d_{\tilde{k}_n}^\dagger|0\rangle + c\leftrightarrow d\big]\Bigg)\end{aligned} \tag{A61}$$

and the second term yields

$$\begin{aligned}&\int dX\,\langle 0|c_{p_1}\cdots c_{p_n}c_{\tilde{p}_1}d_{\tilde{p}_2}\cdots d_{\tilde{p}_n}c_{k_1}^\dagger\dots c_{k_n}^\dagger c_{\tilde{k}_1}^\dagger d_{\tilde{k}_2}^\dagger\dots d_{\tilde{k}_n}^\dagger|0\rangle \\ &= \int dX\Bigg([c_{\tilde{p}_1}, c_{\tilde{k}_1}^\dagger](n-1)!\prod_{i=2}^{n}[d_{\tilde{p}_i}, c_{\tilde{k}_i}^\dagger]n!\prod_{i=1}^{n}[c_{p_i}, c_{k_i}^\dagger] + n[c_{\tilde{p}_1}, c_{k_1}^\dagger]n[c_{p_1}, c_{\tilde{k}_1}^\dagger](n-1)!\prod_{i=2}^{n}[d_{\tilde{p}_i}, c_{\tilde{k}_i}^\dagger](n-1)!\prod_{i=2}^{n}[c_{p_i}, c_{k_i}^\dagger]\Bigg) \\ &= \frac{1}{n} + I_{2n}.\end{aligned} \tag{A62}$$

Putting everything together,

$$\langle\psi_\varphi^{(0)}|\dot{\psi}_\varphi^{(0)}\rangle = -\frac{N}{2}\eta\left(1 + \frac{N}{2}I_N\right) + O(\eta^2), \tag{A63}$$

where we used that $n = N/2$. A similar derivation yields

$$\langle\dot{\psi}_\varphi^{(0)}|\dot{\psi}_\varphi^{(0)}\rangle = \frac{N^2}{2}I_N + N + O(\eta^2) \tag{A64}$$

and hence

$$F_Q\big[\psi_\varphi^{(0)}\big] \approx F_Q[\psi_\varphi] - \frac{N^2\eta I_N}{4}, \tag{A65}$$

where $F_Q[\psi_\varphi]$ is the QFI without losses and we considered only dominant terms in η and N. Note that this is a conservative bound, since we expect the other terms in Eq. (A52), where more photons have been lost, to also contribute to the QFI.

[1] V. Giovannetti, S. Lloyd, and L. Maccone, Advances in quantum metrology, Nat. Photon. **5**, 222 (2011).

[2] G. Tóth and I. Apellaniz, Quantum metrology from a quantum information science perspective, J. Phys. A: Math. Theor. **47**, 424006 (2014).

[3] J. P. Dowling and K. P. Seshadreesan, Quantum optical technologies for metrology, sensing, and imaging, J. Lightwave Technol. **33**, 2359 (2015).

[4] R. Demkowicz-Dobrzański, M. Jarzyna, and J. Kołodyński, Quantum limits in optical interferometry, in *Progress in Optics* (Elsevier, Amsterdam, 2015), pp. 345–435.

[5] J. Estève, C. Gross, A. Weller, S. Giovanazzi, and M. K. Oberthaler, Squeezing and entanglement in a Bose-Einstein condensate, Nature (London) **455**, 1216 (2008).

[6] M. F. Riedel, P. Böhi, Y. Li, T. W. Hänsch, A. Sinatra, and P. Treutlein, Atom-chip-based generation of entanglement for quantum metrology, Nature (London) **464**, 1170 (2010).

[7] C. F. Ockeloen, R. Schmied, M. F. Riedel, and P. Treutlein, Quantum Metrology with a Scanning Probe Atom Interferometer, Phys. Rev. Lett. **111**, 143001 (2013).

[8] A. Louchet-Chauvet, J. Appel, J. J. Renema, D. Oblak, N. Kjaergaard, and E. S. Polzik, Entanglement-assisted atomic clock beyond the projection noise limit, New J. Phys. **12**, 065032 (2010).

[9] J. Appel, P. J. Windpassinger, D. Oblak, U. B. Hoff, N. Kjaergaard, and E. S. Polzik, Mesoscopic atomic entanglement for precision measurements beyond the standard quantum limit, Proc. Natl. Acad. Sci. USA **106**, 10960 (2009).

[10] T. Fernholz, H. Krauter, K. Jensen, J. F. Sherson, A. S. Sørensen, and E. S. Polzik, Spin Squeezing of Atomic Ensembles via Nuclear-electronic Spin Entanglement, Phys. Rev. Lett. **101**, 073601 (2008).

[11] W. Wasilewski, K. Jensen, H. Krauter, J. J. Renema, M. V. Balabas, and E. S. Polzik, Quantum Noise Limited and Entanglement-assisted Magnetometry, Phys. Rev. Lett. **104**, 133601 (2010).

[12] G. Tóth and M. W. Mitchell, Generation of macroscopic singlet states in atomic ensembles, New J. Phys. **12**, 053007 (2010).

[13] N. Behbood, F. M. Ciurana, G. Colangelo, M. Napolitano, G. Tóth, R. J. Sewell, and M. W. Mitchell, Generation of Macroscopic Singlet States in a Cold Atomic Ensemble, Phys. Rev. Lett. **113**, 093601 (2014).

[14] C. M. Caves, Quantum-mechanical noise in an interferometer, Phys. Rev. D **23**, 1693 (1981).

[15] H. Vahlbruch, M. Mehmet, K. Danzmann, and R. Schnabel, Detection of 15 db Squeezed States of Light and their Application for the Absolute Calibration of Photoelectric Quantum Efficiency, Phys. Rev. Lett. **117**, 110801 (2016).

[16] U. L. Andersen, T. Gehring, C. Marquardt, and G. Leuchs, 30 years of squeezed light generation, Phys. Scr. **91**, 053001 (2016).

[17] J. J. Bollinger, W. M. Itano, D. J. Wineland, and D. J. Heinzen, Optimal frequency measurements with maximally correlated states, Phys. Rev. A **54**, R4649 (1996).

[18] M. J. Holland and K. Burnett, Interferometric Detection of Optical Phase Shifts at the Heisenberg Limit, Phys. Rev. Lett. **71**, 1355 (1993).

[19] M. W. Mitchell, J. S. Lundeen, and A. M. Steinberg, Super-resolving phase measurements with a multiphoton entangled state, Nature (London) **429**, 161 (2004).

[20] T. Nagata, R. Okamoto, J. L. O'brien, K. Sasaki, and S. Takeuchi, Beating the standard quantum limit with four-entangled photons, Science **316**, 726 (2007).

[21] S. Slussarenko, M. M. Weston, H. M. Chrzanowski, L. K. Shalm, V. B. Verma, S. W. Nam, and G. J. Pryde, Unconditional violation of the shot-noise limit in photonic quantum metrology, Nat. Photon. **11**, 700 (2017).

[22] M. Dakna, J. Clausen, L. Knöll, and D.-G. Welsch, Generation of arbitrary quantum states of traveling fields, Phys. Rev. A **59**, 1658 (1999).

[23] X.-L. Wang, L.-K. Chen, W. Li, H.-L. Huang, C. Liu, C. Chen, Y.-H. Luo, Z.-E. Su, D. Wu, Z.-D. Li, H. Lu, Y. Hu, X. Jiang, C.-Z. Peng, L. Li, N.-L. Liu, Yu.-A. Chen, C.-Y. Lu, and J.-W. Pan, Experimental Ten-Photon Entanglement, Phys. Rev. Lett. **117**, 210502 (2016).

[24] E. Vetsch, D. Reitz, G. Sagué, R. Schmidt, S. T. Dawkins, and A. Rauschenbeutel, Optical Interface Created by Laser-Cooled Atoms Trapped in the Evanescent Field Surrounding an Optical Nanofiber, Phys. Rev. Lett. **104**, 203603 (2010).

[25] J. D. Thompson, T. G. Tiecke, N. P. de Leon, J. Feist, A. V. Akimov, M. Gullans, A. S. Zibrov, V. Vuletic, and M. D. Lukin, Coupling a single trapped atom to a nanoscale optical cavity, Science **340**, 1202 (2013).

[26] A. Goban, C.-L. Hung, S.-P Yu, J. D. Hood, J. A. Muniz, J. H. Lee, M. J. Martin, A. C. McClung, K. S. Choi, D. E. Chang, O. Painter, and H. J. Kimble, Atom-light interactions in photonic crystals, Nat. Commun. **5**, 3808 (2014).

[27] S. Faez, P. Türschmann, H. R. Haakh, S. Götzinger, and V. Sandoghdar, Coherent Interaction of Light and Single Molecules in a Dielectric Nanoguide, Phys. Rev. Lett. **113**, 213601 (2014).

[28] P. Lodahl, S. Mahmoodian, and S. Stobbe, Interfacing single photons and single quantum dots with photonic nanostructures, Rev. Mod. Phys. **87**, 347 (2015).

[29] A. Sipahigil, R. E. Evans, D. D. Sukachev, M. J. Burek, J. Borregaard, M. K. Bhaskar, C. T. Nguyen, J. L. Pacheco, H. A. Atikian, C. Meuwly *et al.*, An integrated diamond nanophotonics platform for quantum optical networks, Science **354**, 847 (2016).

[30] N. V. Corzo, B. Gouraud, A. Chandra, A. Goban, A. S. Sheremet, D. V. Kupriyanov, and J. Laurat, Large Bragg Reflection from One-dimensional Chains of Trapped Atoms Near a Nanoscale Waveguide, Phys. Rev. Lett. **117**, 133603 (2016).

[31] H. L. Sørensen, J.-B. Béguin, K. W. Kluge, I. Iakoupov, A. S. Sørensen, J. H. Müller, E. S. Polzik, and J. Appel, Coherent Backscattering of Light Off One-dimensional Atomic Strings, Phys. Rev. Lett. **117**, 133604 (2016).

[32] P. Solano, P. Barberis-Blostein, F. K. Fatemi, L. A. Orozco, and S. L. Rolston, Super-radiance reveals infinite-range dipole interactions through a nanofiber, Nat. Commun. **8**, 1857 (2017).

[33] R. H. Dicke, Coherence in spontaneous radiation processes, Phys. Rev. **93**, 99 (1954).

[34] D. Porras and J. I. Cirac, Collective generation of quantum states of light by entangled atoms, Phys. Rev. A **78**, 053816 (2008).

[35] A. González-Tudela, V. Paulisch, D. E. Chang, H. J. Kimble, and J. I. Cirac, Deterministic Generation of Arbitrary Photonic States Assisted by Dissipation, Phys. Rev. Lett. **115**, 163603 (2015).

[36] V. Paulisch, A. González-Tudela, H. J. Kimble, and J. I. Cirac, Heralded multiphoton states with coherent spin interactions in waveguide QED, New J. Phys. **19**, 043004 (2017).

[37] A. González-Tudela, V. Paulisch, H. J. Kimble, and J. I. Cirac, Efficient Multiphoton Generation in Waveguide Quantum Electrodynamics, Phys. Rev. Lett. **118**, 213601 (2017).

[38] M. J. Hartmann, F. G. S. L. Brandão, and M. B. Plenio, Quantum many-body phenomena in coupled cavity arrays, Laser Photon. Rev. **2**, 527 (2008).

[39] Y. Ota, S. Iwamoto, N. Kumagai, and Y. Arakawa, Spontaneous Two-photon Emission from a Single Quantum Dot, Phys. Rev. Lett. **107**, 233602 (2011).

[40] C. W. Helstrom, *Quantum Detection and Estimation Theory* (Elsevier Science, Amsterdam, 1976).

[41] A. S. Holevo, *Probabilistic and Statistical Aspects of Quantum Theory (Statistics & Probability) (English and Russian Edition)* (Elsevier Science, Amsterdam, 1982).

[42] S. L. Braunstein and C. M. Caves, Statistical Distance and the Geometry of Quantum States, Phys. Rev. Lett. **72**, 3439 (1994).

[43] L. Pezzé and A. Smerzi, Ultrasensitive Two-mode Interferometry with Single-mode Number Squeezing, Phys. Rev. Lett. **110**, 163604 (2013).

[44] R. A. Campos, C. C. Gerry, and A. Benmoussa, Optical interferometry at the Heisenberg limit with twin Fock states and parity measurements, Phys. Rev. A **68**, 023810 (2003).

[45] H. F. Hofmann, All path-symmetric pure states achieve their maximal phase sensitivity in conventional two-path interferometry, Phys. Rev. A **79**, 033822 (2009).

[46] S. Olivares and M. G. A. Paris, Optimized interferometry with Gaussian states, Opt. Spectrosc. **103**, 231 (2007).

[47] L. Pezzé and A. Smerzi, Entanglement, Nonlinear Dynamics, and the Heisenberg Limit, Phys. Rev. Lett. **102**, 100401 (2009).

[48] P. Hyllus, O. Gühne, and A. Smerzi, Not all pure entangled states are useful for sub-shot-noise interferometry, Phys. Rev. A **82**, 012337 (2010).

[49] M. Oszmaniec, R. Augusiak, C. Gogolin, J. Kołodyński, A. Acín, and M. Lewenstein, Random Bosonic States for Robust Quantum Metrology, Phys. Rev. X **6**, 041044 (2016).

[50] G. W. Gardiner and P. Zoller, *Quantum Noise*, 2nd ed. (Springer-Verlag, Berlin, 2000).

[51] This simplification can be applied to any wave function that is symmetrized by summing over all permutations as in (9).

[52] B. M. Escher, R. L. de Matos Filho, and L. Davidovich, General framework for estimating the ultimate precision limit in noisy quantum-enhanced metrology, Nat. Phys. **7**, 406 (2011).

[53] R. Demkowicz-Dobrzański, J. Kołodyński, and M. Guţă, The elusive Heisenberg limit in quantum-enhanced metrology, Nat. Commun. **3**, 1063 (2012).

[54] M. Perarnau-Llobet, A. González-Tudela, and J. I. Cirac (unpublished).

[55] S. Knysh, V. N. Smelyanskiy, and G. A. Durkin, Scaling laws for precision in quantum interferometry and the bifurcation landscape of the optimal state, Phys. Rev. A **83**, 021804(R) (2011).

[56] F. Haas, J. Volz, R. Gehr, J. Reichel, and J. Estève, Entangled states of more than 40 atoms in an optical fiber cavity, Science **344**, 180 (2014).

[57] M. A. Norcia, M. N. Winchester, J. R. K. Cline, and J. K. Thompson, Superradiance on the millihertz linewidth strontium clock transition, Sci. Adv. **2**, e1601231 (2016).

[58] M. Hosseini, Y. Duan, K. M. Beck, Yu.-T. Chen, and V. Vuletić, Cavity Cooling of Many Atoms, Phys. Rev. Lett. **118**, 183601 (2017).

[59] J. Kim, D. Yang, S.-H. Oh, and K. An, Coherent single-atom superradiance, Science **359**, 662 (2017).

[60] A. N. Boto, P. Kok, D. S. Abrams, S. L. Braunstein, C. P. Williams, and J. P. Dowling, Quantum Interferometric Optical Lithography: Exploiting Entanglement to Beat the Diffraction Limit, Phys. Rev. Lett. **85**, 2733 (2000).